Hand/Eye-Vergence システムに基いて奥行き方向に移動する物体へのビジュアルサーボ

○寇　ギョウ郡　　田　宏志　　見浪　護（岡山大学）

Visual Sevroing to Longitudinally Moving Obejct Based on Hand/Eye-Vergence Dual Cameras System

∗Y. Kou　H. Tian　M. Minami (Okayama University)

Abstract– Visual servoing to moving target with hand-eye cameras fixed at hand is inevitably affected by robot's dynamical oscillations, therefore it is difficult for the fixed-hand-eye robot to keep target object at the center of cameras' view, since nonlinear dynamical effects of whole manipulator and intensive dynamical coupling of each link stand against keeping consistent servoing accuracy. To improve the defects of the fixed-hand-eye system, hand-eye-vergence system has attracted attention—left and right cameras' directions could be rotated to observe and keep the target object be recognized at the center of camera images, reducing the influences of aberration of camera lens. On top of this, the longitudinal moving object is more difficult to be recognized than the lateral one, because the image change is less than the real motion of the object. By using "3D Move on Sensing (3D-MoS)", which is a method to control robot's 3D pose (position and orientation) by using detected 3D Pose through dual cameras system. This research confirmed that the hand-eye-vergence system can improve the observability and trackability on visual servoing in camera-depth direction.

Key Words: Visual Servoing, Eye-vergence, 3D-MoS

1 Introduction

Visual servoing is a control method to control the motion of robot. By incorporating visual information obtained from visual sensor[1]-[4] with the feedback loop, visual servoing is expected to be able to allow the robot adapt the changing or unknown environment. Some methods have been proposed already to improve the observation abilities of the robot, for instance by using stereo cameras[5], multiple cameras[6], and a method with one camera fixed on the end-effector, the other done in the workspace[7]. However these methods obtain different views to observe the object by increasing the number of cameras, leaving the system less adaptive for changing environment.

Even through there have been plenty try concerning on the visual servoing about tracking object, however the final goal of the visual servoing was been considered as realize the end-effector approaching to the target then work on it, for instance grasping. In this case, the desired relation between the cameras and the object should be time varying, for this reason, the eye-vergence camera system is a settlement to keep suitable viewpoint on the target all the time during the approaching visual servoing, utilizing the changeable cameras' eye direction in order to keep the target been recognized at the center of the image.

The other merit of eye-vergence is concerning dynamical effects to keep tracking a moving target in the camera's view. For example, when people keep tracking a moving object, they may catch up to the object in case of the object moving slowly, but when the object become to move faster and faster, human's face cannot be kept positioned squarely to the object, while human's eye can still keep staring at the object because of its small mass and inertial moment. Needless to say in visual servoing application, keeping closed loop of visual feedback is vital from a view point of closed loop control stability.

By a previous work, it has been clarified that the eye-vergence system has superior stability and trackability performances in pose tracking dynamical motions in lateral direction. However, pose tracking of longitudinally moving object has a difficulty for depth distance to be estimated than laterally moving one, because the image changes becomes less in cameras' view against when the object's motion in real world. In this report, we conduct some visual servoing experiments about object's longitudinal movement by using fixed-camera system and confirmed that eye-vergence system can perform well in longitudinal tracking. From the experiment results, we verified about the error of object estimation by showing the action of GA in time-domain during visual servoing.

2 3D Pose Tracking Method

In this paper,we take a rectangular solid block as an example of the target to explain The 3D Pose Tracking Method.The shape and color of the solid block is assumed to be known.Other different kinds of targets can also be measured by model-based matching strategy if their character is given.

2.1 Kinematics of Stereo-Vision

We utilize perspective projection as projection transformation. Fig. 1 shows the coordinate system of the dual-eyes vision system. The target object's coordinate system is represented by Σ_M and image coordinate systems of the left and right cameras are represented by Σ_{IL} and Σ_{IR}. A point i on the target

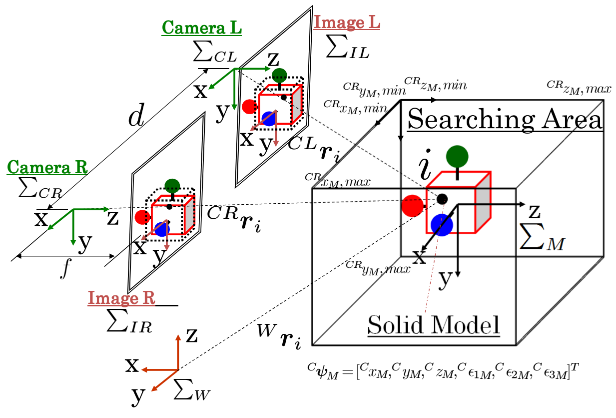

Fig. 1: Coordinate systems of dual eyes

can be described using these coordinates and homogeneous transformation matrices. At first, a homogeneous transformation matrix from right camera coordinates, Σ_{CR} to Σ_M is defined as ${}^{CR}\boldsymbol{T}_M$. And an arbitrary point i on the target object in Σ_{CR} and Σ_M is defined ${}^{CR}\boldsymbol{r}_i$ and ${}^{M}\boldsymbol{r}_i$. Then ${}^{CR}\boldsymbol{r}_i$ is,

$${}^{CR}\boldsymbol{r}_i = {}^{CR}\boldsymbol{T}_M \, {}^{M}\boldsymbol{r}_i. \tag{1}$$

Where ${}^{M}\boldsymbol{r}_i$ is predetermined fixed vectors. Using a homogeneous Σ_W to Σ_{CR}, i.e., ${}^{W}\boldsymbol{T}_{CR}$, then ${}^{W}\boldsymbol{r}_i$ is got as,

$${}^{W}\boldsymbol{r}_i = {}^{W}\boldsymbol{T}_{CR} \, {}^{CR}\boldsymbol{r}_i. \tag{2}$$

The position vector of i point in right image coordinates, ${}^{IR}\boldsymbol{r}_i$ is described by using projection matrix $\boldsymbol{P}$ of camera as,

$${}^{IR}\boldsymbol{r}_i = \boldsymbol{P} \, {}^{CR}\boldsymbol{r}_i. \tag{3}$$

By the same way as above.

$${}^{CL}\boldsymbol{r}_i = {}^{CL}\boldsymbol{T}_M \, {}^{M}\boldsymbol{r}_i. \tag{4}$$

$${}^{W}\boldsymbol{r}_i = {}^{W}\boldsymbol{T}_{CL} \, {}^{CL}\boldsymbol{r}_i. \tag{5}$$

$${}^{IL}\boldsymbol{r}_i = \boldsymbol{P} \, {}^{CL}\boldsymbol{r}_i. \tag{6}$$

Then position vectors projected in the Σ_{IR} and Σ_{IL} of arbitrary point i on target object can be described ${}^{IR}\boldsymbol{r}_i$ and ${}^{IL}\boldsymbol{r}_i$. Here, position and orientation of Σ_M based on Σ_{CR} has been defined as ${}^{CR}\boldsymbol{\psi}_M$. Then Eq.(3), Eq.(6) are rewritten as,

$$\begin{cases} {}^{IR}\boldsymbol{r}_i = \boldsymbol{f}_R({}^{CR}\boldsymbol{\psi}_M, \ {}^{M}\boldsymbol{r}_i) \\ {}^{IL}\boldsymbol{r}_i = \boldsymbol{f}_L({}^{CL}\boldsymbol{\psi}_M, \ {}^{M}\boldsymbol{r}_i). \end{cases} \tag{7}$$

This relation connects the arbitrary points on the object and projected points on the left and right images corresponding to a 3D pose ${}^{CR}\boldsymbol{\psi}_M$ of the object. The measurement of ${}^{CR}\boldsymbol{\psi}_M(t)$ in real time will be solved by consistent convergence of a matching model to the target object by a “Real-Time Multi-Step GA”.

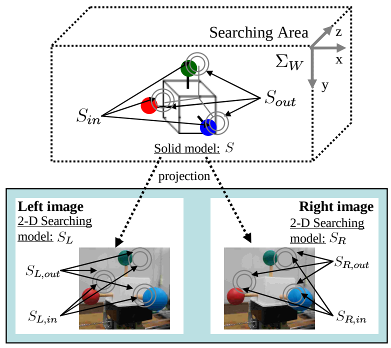

Fig. 2: Definition of a solid model and left/right searching models

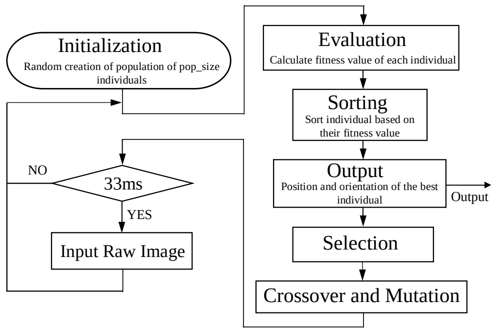

Fig. 3: Flow chart of Real-Time Multi-Step GA recognition

2.2 Model-based matching

The 3D solid model is shown in Fig. 2. The model is constituted of inside space S_{in} and outside space S_{out}. The left and right 2D searching models, named S_L and S_R, are shown in Fig. 2(on the bottom). Supposing there are distributed solid models in the searching space in Σ_W, each has its own pose ${}^{CR}\boldsymbol{\psi}_M$, ${}^{CL}\boldsymbol{\psi}_M$. To determine which solid model is most close to the real target, a correlation function used fitness function in GA is defined for evaluation. Here, we use color information to search for the target object in the images. In order to evaluate difference of hue value between the object and the searching model. The hue value of right image at the position ${}^{IR}\boldsymbol{r}_i$ is expressed as $p({}^{IR}\boldsymbol{r}_i)$, and the hue value of left image at the position ${}^{IL}\boldsymbol{r}_i$ is expressed as $p({}^{IL}\boldsymbol{r}_i)$.

$$\begin{aligned} F({}^{C}\boldsymbol{\psi}_M) = & \Bigg\{ \Bigg(\sum_{{}^{IR}\boldsymbol{r}_i \in S_{R,in}({}^{CR}\boldsymbol{\psi}_M)} p({}^{IR}\boldsymbol{r}_i) - \sum_{{}^{IR}\boldsymbol{r}_i \in S_{R,out}({}^{CR}\boldsymbol{\psi}_M)} p({}^{IR}\boldsymbol{r}_i) \Bigg) \\ & + \Bigg(\sum_{{}^{IL}\boldsymbol{r}_i \in S_{L,in}({}^{CL}\boldsymbol{\psi}_M)} p({}^{IL}\boldsymbol{r}_i) - \sum_{{}^{IL}\boldsymbol{r}_i \in S_{L,out}({}^{CL}\boldsymbol{\psi}_M)} p({}^{IL}\boldsymbol{r}_i) \Bigg) \Bigg\} /2 \\ = & \ \{F_R({}^{CR}\boldsymbol{\psi}_M) + F_L({}^{CL}\boldsymbol{\psi}_M)\}/2 \end{aligned} \tag{8}$$

Eq.(8) shows the fitness function that calculate the correlation function between the search model and image. When the searching model fits to the target object being imaged in the right and left images, then the fitness function $F({}^{C}\boldsymbol{\psi}_M)$ gives maximum value,

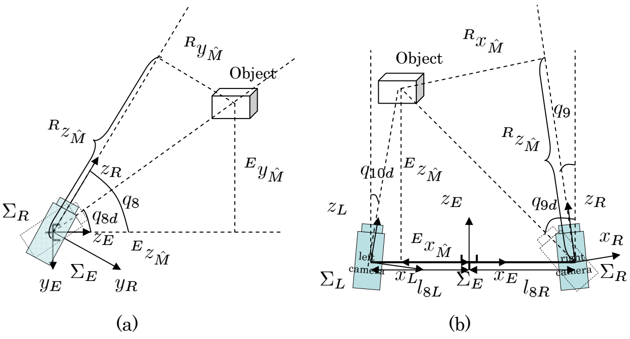

Fig. 4: Calculation of tilt and pan angles

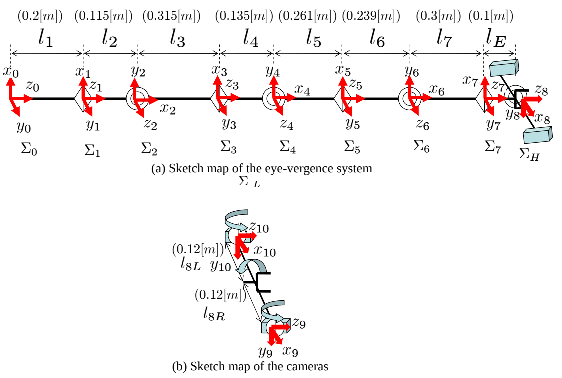

Fig. 5: Frame structure of manipulator

i.e., $F = 1$.
Therefore the problem of finding a target object and detecting its position/orientation can be converted to searching ${}^{C}\boldsymbol{\psi}_M$ that maximizes $F({}^{C}\boldsymbol{\psi}_M)$. We solve this optimization problem by GA. The genes of GA representing possible pose solution ${}^{C}\boldsymbol{\psi}_M$ is defined as,

$$\underbrace{\overbrace{01\cdots01}^{t_x}}_{12bit}\underbrace{\overbrace{00\cdots01}^{t_y}}_{12bit}\underbrace{\overbrace{11\cdots01}^{t_z}}_{12bit}\underbrace{\overbrace{01\cdots01}^{\epsilon_1}}_{12bit}\underbrace{\overbrace{01\cdots11}^{\epsilon_2}}_{12bit}\underbrace{\overbrace{01\cdots10}^{\epsilon_3}}_{12bit}.$$

The 72 bits of gene refers to the range of the searching area: $-150 \leq t_x \leq 150[mm]$, $0 \leq t_y \leq 300[mm]$, $650 \leq t_z \leq 950[mm]$, and $-0.3 \leq \epsilon_1, \epsilon_2, \epsilon_3 \leq 0.3$, where ϵ_i is defined as quaternion and represents almost the same range of $-54 \leq roll, pitch, yaw \leq 54[deg]$.
Although GA has been applied to a number of robot control systems [13], it has not been yet applied to a robot manipulator control system to track a target in 3D space with unpredictable movement in real time, since the general GA method costs much time until its convergence. So here, for real-time visual control purposes, we have employed GA in a way that we denoted as "Real-Time Multi-Step GA" evolution. This means that the GA evolutional iteration is applied one time to the newly input image. While using the elitist model of the GA, the most accurate pose of a target can be detect in every new image by the pose of the gene with highest fitness value. In addition, this feature happens to be favorable for real-time visual recognition. The flow chart of the Real-Time Multi-

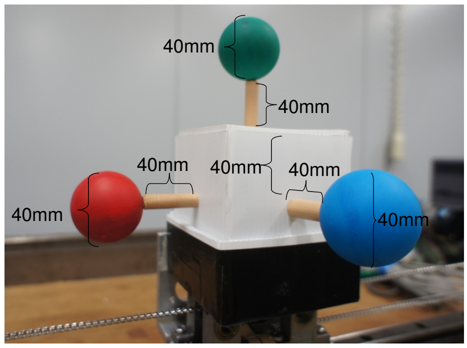

Fig. 6: 3D marker

step GA process is shown in Fig. 3. The pose of the best gene is output in every newly input image on a on-line measurement result, to be used as command value to the manipulator's controller. Thereby real-time visual servoing can be performed. Our previous research has confirmed the 2D recognition method enabled a eye-in-hand robot manipulator to catch a swimming fish by a net equipped at the hand [11]. Fig. 3 shows that the image inputting process is included in the GA iteration process seeking for the potential solution, i.e., toward the target. That is, the evolving speed to the solution in the image should be faster than the speed of the target object in the successively input images, for the success of real-time recognition by "Real-Time Multi-Step GA."

3 Hand & Eye Visual Servoing Controller

3.1 Hand Visual Servoing Controller

The block diagram of our proposed hand & eye-vergence visual servoing controller is shown in Fig. 8. The hand-visual servoing is the outer loop. Based on the above analysis of the desired-trajectory generation, the desired hand velocity ${}^{W}\dot{\boldsymbol{r}}_d$ is calculated as,

$${}^{W}\dot{\boldsymbol{r}}_d = \boldsymbol{K}_{P_p}{}^{W}\boldsymbol{r}_{E,Ed} + \boldsymbol{K}_{V_p}{}^{W}\dot{\boldsymbol{r}}_{E,Ed}, \quad (9)$$

where ${}^{W}\boldsymbol{r}_{E,Ed}$, ${}^{W}\dot{\boldsymbol{r}}_{E,Ed}$ can be calculated from ${}^{E}\boldsymbol{T}_{Ed}$ and ${}^{E}\dot{\boldsymbol{T}}_{Ed}$. $\boldsymbol{K}_{P_p}$ and $\boldsymbol{K}_{V_p}$ are positive definite matrix to determine PD gain.

The desired hand angular velocity ${}^{W}\boldsymbol{\omega}_d$ is calculated as,

$${}^{W}\boldsymbol{\omega}_d = \boldsymbol{K}_{P_o}{}^{W}\boldsymbol{R}_E{}^{E}\Delta\boldsymbol{\epsilon} + \boldsymbol{K}_{V_o}{}^{W}\boldsymbol{\omega}_{E,Ed}, \quad (10)$$

where ${}^{E}\Delta\boldsymbol{\epsilon}$ is a quaternion error [12] calculated from the pose tracking result, and ${}^{W}\boldsymbol{\omega}_{E,Ed}$ can be computed by transforming the base coordinates of ${}^{E}\boldsymbol{T}_{Ed}$ and ${}^{E}\dot{\boldsymbol{T}}_{Ed}$ from Σ_E to Σ_W. Also, $\boldsymbol{K}_{P_o}$ and $\boldsymbol{K}_{V_o}$ are suitable feedback matrix gains. We define the desired hand pose as ${}^{W}\boldsymbol{\psi}_d^T = [{}^{W}\boldsymbol{r}_d^T, {}^{W}\boldsymbol{\epsilon}_d^T]^T$

The desired joint variable $\boldsymbol{q}_{Ed} = [q_{1d}, \ldots, q_{7d}]^T$ and $\dot{\boldsymbol{q}}_{Ed}$ is obtained by

$$\boldsymbol{q}_{Ed} \quad = \quad \boldsymbol{f}^{-1}({}^{W}\boldsymbol{\psi}_d^T) \quad (11)$$

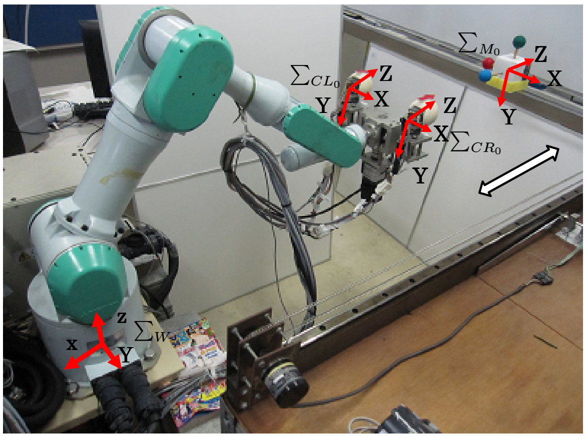

Fig. 7: Object and the visual-servoing system

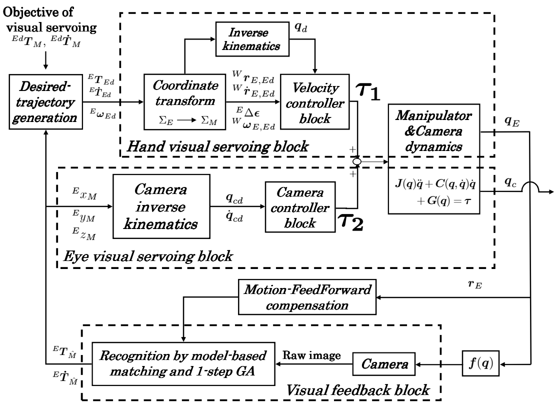

Fig. 8: Block diagram of the hand visual servoing system

$$\dot{\boldsymbol{q}}_{Ed} \quad = \quad \boldsymbol{J}_E^+(\boldsymbol{q}) \begin{bmatrix} {}^W\dot{\boldsymbol{r}}_d \\ {}^W\boldsymbol{\omega}_d \end{bmatrix} \tag{12}$$

where $\boldsymbol{f}^{-1}({}^W\boldsymbol{\psi}_d^T)$ is the inverse kinematic function and $\boldsymbol{J}_E^+(\boldsymbol{q})$ is the pseudo-inverse matrix of $\boldsymbol{J}_E(\boldsymbol{q})$, and $\boldsymbol{J}_E^+(\boldsymbol{q}) = \boldsymbol{J}_E^T(\boldsymbol{J}_E\boldsymbol{J}_E^T)^{-1}$. In this report, we made q_1 is 0, and used the inverse kinematics to calculate all joint angles. It can solve the redundancy problem. Meanwhile we took a controller to make the joint of angles approximately as the desired joint angles. So we defined the formula of the desired joint angles in the new controller as

$$\dot{\boldsymbol{q}}_{Ed} = \boldsymbol{k}_p(\boldsymbol{q}_{Ed} - \boldsymbol{q}_E) + \boldsymbol{J}_E^+(\boldsymbol{q}) \begin{bmatrix} {}^W\dot{\boldsymbol{r}}_d \\ {}^W\boldsymbol{\omega}_d \end{bmatrix} \tag{13}$$

where $\boldsymbol{k}_p$ is P positive gain.

The hardware control system of the velocity-based servo system of PA10 is expressed as

$$\boldsymbol{\tau} = \boldsymbol{K}_{SP}(\boldsymbol{q}_d - \boldsymbol{q}) + \boldsymbol{K}_{SD}(\dot{\boldsymbol{q}}_d - \dot{\boldsymbol{q}}) \tag{14}$$

where $\boldsymbol{K}_{SP}$ and $\boldsymbol{K}_{SD}$ are symmetric positive definite matrices to determine PD gain.

3.2 Eye-vergence Visual Servoing Controller

The eye-vergence visual servoing is the inner loop of the visual servoing system shown in Fig. 8. In this paper, we use two pan-tilt cameras for eye-vergence visual servoing. Here, the positions of cameras are supposed to be fixed on the end-effector. For camera system, q_8 is tilt angle, q_9 and q_{10} are pan angles, and q_8 is common for both cameras.

As it is shown in Fig. 4 (a) and (b), ${}^Ex_{\hat{M}}$, ${}^Ey_{\hat{M}}$, ${}^Ez_{\hat{M}}$ express position of the detected object in the end-effector coordinate. The desired angle of the camera joints are calculated by:

$$q_{8d} \quad = \quad atan2({}^Ey_{\hat{M}}, {}^Ez_{\hat{M}}) \tag{15}$$
$$q_{9d} \quad = \quad atan2(-l_{8R} + {}^Ex_{\hat{M}}, {}^Ez_{\hat{M}}) \tag{16}$$
$$q_{10d} \quad = \quad atan2(l_{8L} + {}^Ex_{\hat{M}}, {}^Ez_{\hat{M}}) \tag{17}$$

where $l_{8L} = l_{8R} = 120[mm]$ that is the camera location.

The controller of eye-visual servoing is given by

$$\dot{q}_{8Cd} \quad = \quad K_P(q_{8d} - q_8) \tag{18}$$
$$\dot{q}_{9Cd} \quad = \quad K_P(q_{9d} - q_9) \tag{19}$$
$$\dot{q}_{10Cd} \quad = \quad K_P(q_{10d} - q_{10}) \tag{20}$$

where K_P are positive control gain.

Because the motion of camera motor is an open loop, we can only make it rotate a certain degree without getting the actual angle during the rotation, which make us cannot get the accurate camera angle. So the desired camera angles are input in every 33ms, and the input is limited to a certain value.

4 Experiment Of Hand Eye-Vergence Visual Servoing

4.1 Experimental system

To verify the effectiveness of the hand & eye visual servoing system through real robot, we used a robot, PA-10 robot arm that has a 7-DoF robot arm manufactured by Mitsubishi Heavy Industries. Two rotatable cameras mounted on the end-effector are FCB-1X11A manufactured by Sony Industries. The frame frequency of stereo cameras is set as 30fps. The image processing board, CT-3001, receiving the image from the CCD camera is connected to the DELL WORKSTATION PWS650 (CPU: Xeon, 2.00 GHz) host computer. The structure of the manipulator and the cameras are shown in Fig. 5 (a) and (b).

The 3D marker as used for the target object in the experiment composes a red ball, a green ball and a blue ball, whose dimension is shown in Fig. 6. The coordinate of the target object and the manipulator in experiment are shown in Fig. 7, the white arrow under the object express the move direction of it.

We did several contrast experiments using fixed camera system, by comparing the data from fixed camera system with the eye-vergence system, to check the track ability of the eye-vergence system. First, we did an experiment in which true object's x, y, z, ε_1, ε_2, ε_3, are assumed to be given to servoing controller. Then we did 3 groups of experiments of frequency response. In these experiments,we made 3-DoF position are recognized by the cameras respectively. For every group, we set ω=1.256 rad/s, ω=0.638 rad/s, and ω=0.314 rad/s separately, which are angular velocities of the object.

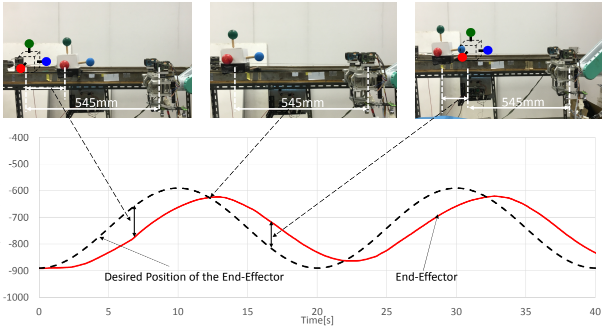

Fig. 9: The relationship of the position of a target and a hand

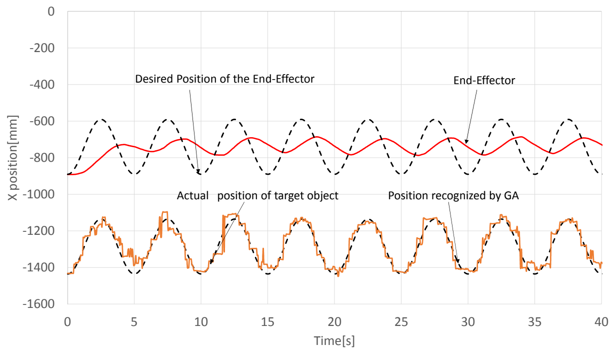

Fig. 10: ω =1.256 (T=5s), Eye-Vergence system

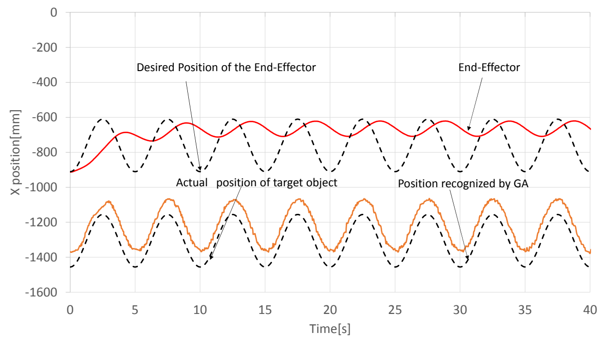

Fig. 11: ω =1.256 (T=5s), Fixed-Camera system

4.2 Experiment condition

The initial hand pose is defined as Σ_{E_0}, and the initial object pose is defined as Σ_{M_0}. The homogeneous transformation matrix from Σ_W to Σ_{E_0} and from Σ_W to Σ_{M_0} are:

$$
{}^{W}\boldsymbol{T}_{E_0} = \begin{bmatrix} 0 & 0 & -1 & -890[mm] \\ 1 & 0 & 0 & 0[mm] \\ 0 & -1 & 0 & 440[mm] \\ 0 & 0 & 0 & 1 \end{bmatrix} \tag{21}
$$

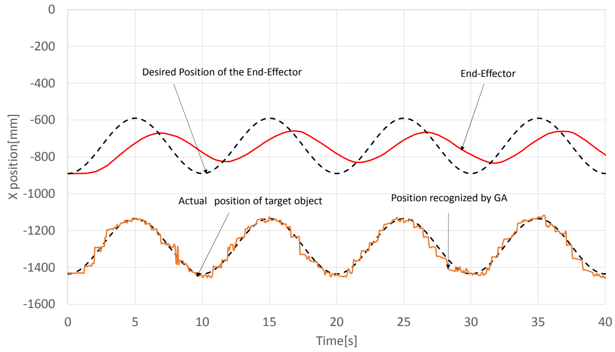

Fig. 12: ω =0.628 (T=10s), Eye-Vergence system

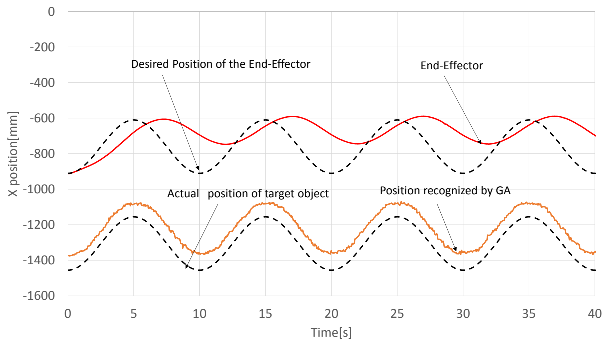

Fig. 13: ω =0.628 (T=10s), Fixed-Camera system

$$
{}^{W}\boldsymbol{T}_{M_0} = \begin{bmatrix} 0 & 0 & -1 & -1435[mm] \\ 1 & 0 & 0 & 0[mm] \\ 0 & -1 & 0 & 440[mm] \\ 0 & 0 & 0 & 1 \end{bmatrix} \tag{22}
$$

The target object move according to the following time function

$$
{}^{M_0}z_M(t) \quad = \quad 150 - 150\cos(\omega t)[mm] \tag{23}
$$

The relation between the object and the desired end-effector is set as:

$$
{}^{Ed}\boldsymbol{\psi}_M = [0, -100[mm], 545[mm], 0, 0, 0] \tag{24}
$$

4.3 Experiment Results

In this experiment conditions, we have carried out some longitudinal frequency response experiments to moving object and the Fig.9 shows the relationship of the position of a target and a hand. We made x-position, 3-Dof position, and 6-Dof position and orientation are estimated by GA respectively, and take the results of 3-Dof position. From each of the results we can see that the eye-vergence system has smaller delay phase which means it will observe the object better. I show the relationship between the GA genes and the object position by the results of the obtained GA. In the Fig.10 and Fig.11,the GA from Eye-Vergence system can estimate target object and track, but the GA from Fixed-Camera is always carrying a delay for about 80[mm], however, even the GA can estimate

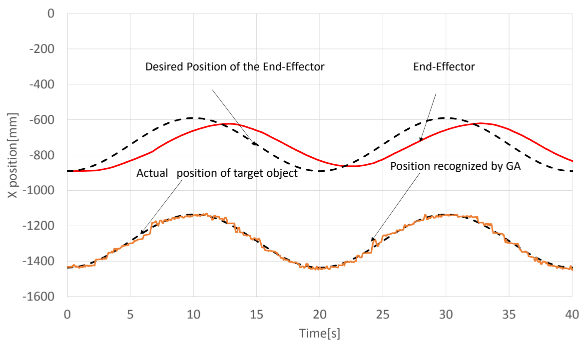

Fig. 14: ω =0.314 (T=20s), Eye-Vergence system

Fig. 15: ω =0.314 (T=20s), Fixed-Camera system

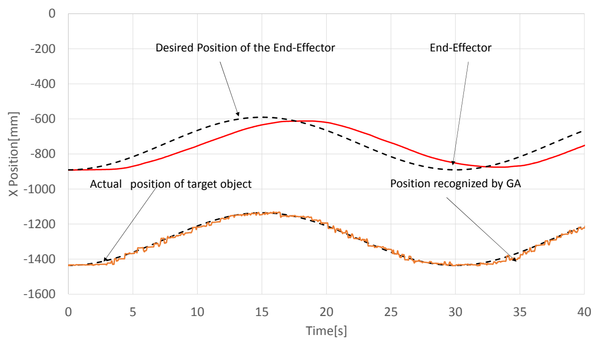

Fig. 16: ω =0.209 (T=30s), Eye-Vergence system

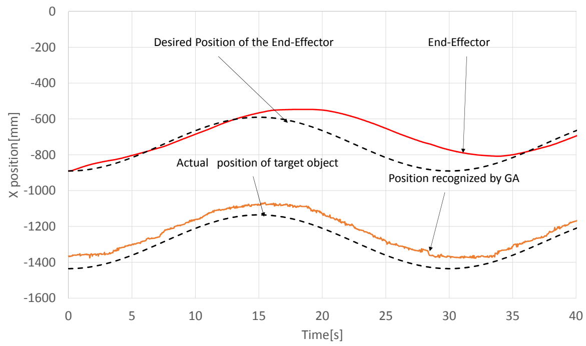

Fig. 17: ω =0.209 (T=30s), Fixed-Camera system

the correct position of the target, but the PA-10 can not track the target object. Because the moment of the inetia of camera is smaller than PA-10's, which is a characteristic of eye-vergence system.Also from the Fig.10 and Fig.11, we can easily find even both two systems' behaviour is poor, the track ability of eye-vergence system is still better than fixed-camera system.

From Fig.12, Fig.13, Fig.14, Fig.15, Fig.16, and Fig.17, we can see with the target object motion is getting slower, the manipulator can track the target with smaller delay. For the GA genes results, the eye-vergence can estimate the target with very small delay, on the contrary, there are always be about 80[mm] error of the fixed-camera system, from which we can conclude that eye-vergence system has a superior performance than fixed-camera system.

5 Conclusion

In this paper, we have carried out some longitudinal frequency response experiments to evaluate the observation and tracking ability on a moving object of visual servoing system. From the experiment results, we can draw a conclusion that the object moving in camera-depth direction can be recognised and Real-Time Multi-step GA can track the correct position in real-time, meaning the Real-Time Multi-step GA is a superior settlement to realize the tracking in real-time. And the authors grasp the real-time estimate tracking error by revealing the relationship between the GA and the target object that was searched in fixed-camera system, by comparing the results, the authors concluded that hand-eye-vergence system has a superior performance than fixed-camera system.

Refences

1) S.Hutchinson, G.Hager, and P.Corke, "A Tutorial on Visual Servo Control", IEEE Trans. on Robotics and Automation, vol. 12, no. 5, pp. 651-670, 1996.

2) P.Y.Oh, and P.K.Allen, "Visual Servoing by Partitioning Degrees of Freedom", IEEE Trans. on Robotics and Automation, vol. 17, no. 1, pp. 1-17, 2001.

3) E.Malis, F.Chaumentte and S.Boudet, "2-1/2-D Visual Servoing", IEEE Trans. on Robotics and Automation, vol. 15, no. 2, pp. 238-250, 1999.

4) P.K.Allen, A.Timchenko, B.Yoshimi, and P.Michelman, "Automated Tracking and Grasping of a Moving object with a Robotic Hand-Eye System", IEEE Trans. on Robotics and Automation, vol. 9, no. 2, pp. 152-165, 1993.

5) Wolfgang Sepp, Stefan Fuchs and Gerd Hirzinger, "Hierarchical Featureless Tracking for Position-Based 6-DoF Visual Servoing", Proceedings of the 2006 IEEE/RSJ Int. Conf. on Intelligent Robotics and Systems (IROS), pp.4310-4315, 2006.

6) Toshifumi Hiramatsu, Takanori Fukao, Keita Kurashiki, Koichi Osuka "Image-based Path Following Control of Mobile Robots with Central Catadioptric Cameras" IEEE International Conference on Robotics and Automation Kobe, Japan, May 12-17, 2009

7) Omar Tahri, Youcef Mezouar "Generic Decoupled Image-Based Visual Servoing for Cameras Obeying the Unified Projection Model" IEEE International Conference on Robotics and Automation Kobe, Japan, May 12-17, 2009

8) W. Song, M. Minami, Y. Mae and S. Aoyagi, " On-line Evolutionary Head Pose Measurement by Feed-forward Stereo Model Matching ", IEEE Int. Conf. on Robotics and Automation (ICRA), pp.4394-4400, 2007.

9) Omar Tahri and Francois Chaumette, “Point-Based and Region-Based Image Moments for Visual Servoing of Planar Objects”, IEEE Tran. on Robotics, vol. 21, no. 6, Dec 2005.

10) Tarek Hamel and Robert Mahony, “Visual Servoing of an Under-Actuated Dynamic Rigid-Body System: An Image-Based Approach”, IEEE Trans. on Robotics and Automation, VOL. 18, NO. 2, APRIL 2002.

11) M.Minami, H.Suzuki, J.Agbanhan, T.Asakura:”Visual Servoing to Fish and Catching Using Global/Local GA Search”, 2001 IEEE/ASME Int. Conf. on Advanced Intelligent Mechatronics Proc., pp.183-188, 2001.

12) W. Song, M. Minami, S. Aoyagi, “On-line Stable Evolutionary Recognition Based on Unit Quaternion Representation by Motion-Feedforward Compensation”, International Journal of Intelligent Computing in Medical Sciences and Image Processing (IC-MED) Vol. 2, No. 2, Page 127-139 (2007).

13) T.Nagata, K.Konishi and H.Zha: ”Cooperative manipulations based on Genetic Algorithms using contact information”, Proceedings of the International Conference on Intelligent Robots and Systems, pp.400-5, 1995